Study the Performance of Bi 2 S 3 Based Solar Cells with various Electron Transport Layers: A Numerical Investigation using DFT and SCAPS-1D

Vishvas Kumar
krvis254@gmail.com

SRM Institute of Science and Technology

Research Article

Keywords: Bi2S3 , DFT, SCAPS-1D and ETL

Posted Date: June 2nd, 2025

DOI: https://doi.org/10.21203/rs.3.rs-6738949/v1

Additional Declarations: No competing interests reported.

Study the Performance of Bi_2S_3-Based Solar Cells with various Electron Transport Layers: A Numerical Investigation using DFT and SCAPS-1D

Vishvas Kumar
krvis254@gmail.com
Department of Electronics and communication Engineering, SRM Institute of Science and Technology, Kattankulathur - 603203,Tamil Nadu, India

Abstract

Due to increase in demand of renewable energy, the new earth abundant, nontoxic, and stable material require for photovoltaic (PV) development. In this point of view, the Bi_2S_3 compound semiconductor have gained a lot of attention as a new absorber layer for thin film photovoltaic applications. In this work, Quantum Espresso (QE) Burai was used to carry out density functional theory (DFT) for Bi_2S_3 to optimize and calculate its structural, electronic band structure, and density of states (DOS). The calculated bandgap of the Bi_2S_3 absorber layer using the PBE approach of QE was 1.25 eV. Additionally, a Bi_2S_3-based solar cell structure (ITO/ETL/ Bi_2S_3/Au) was designed in SCAPS-1D with four (CdS, ZnS, SnS_2, In2S_3) different electron transport layers (ETL). In this structure, ZnS shows the best ETL after optimization with a maximum efficiency of 25.21%. The effect of the ETL and absorber thickness, shunt, series resistance, and operating temperature was evaluated for all four ETL layers, along with their corresponding recombination rate, generation rate, current density–voltage, capacitance–voltage, and quantum efficiency characteristics, which were also calculated using SCAPS-1D.

Keywords:-*Bi_2S_3 , DFT, SCAPS-1D and ETL*

1. Introduction

The commercialised thin film solar cell, like copper indium gallium selenide (CIGS) and cadmium telluride (CdTe) have shown promising levels of efficiency up to 22.1 and 23.5%, respectively [1]. However, there are various constraints to their large-scale use. Firstly, CdTe consists of the rare earth element tellurium (Te), which restricts its large-scale manufacturing and deployments. Additionally, Cadmium is toxic, leading to environmental danger during manufacturing and dumping. Moreover, CIGS consists of indium and gallium, which are costlier and have limited availability on earth. These constraints have encouraged research into substitute absorber materials for thin film solar cells.

As a possible alternative, materials like tri-chalcogenides, specifically Sb_2S_3 and Bi_2S_3, have attracted and gained much attention from researchers. Furthermore, Bi_2S_3 and Sb_2S_3 possess various advantages compared to other materials. They are earth-abundant, non-toxic, low-cost, and eco-friendly. In addition, they exhibit outstanding chemical stability and can be processed using a cost-effective solution-based method. Nanocrystal-based sensitizers of Bi_2S_3 and Sb_2S_3 have been effectively employed in nano heterojunction solar cells and photodetectors[2]. In the case of thin film-based cells using metal chalcogenides X_2Y_3 compounds, where X is As, Bi, Sb, and Y is Se, S, Te, have been studied with great interest due to their suitable band gap, optical, and electronic properties. Among these metal chalcogenides, Sb_2S_3, which has a band gap energy ranging from 1.7 to 1.8 eV, has been extensively studied because of its nontoxic behaviour and excellent photosensitivity, the reported practical PCE is greater than 8% in lab scale [3] and the reported theoretical efficiency of numerically simulated Sb_2S_3 absorber based solar cell is 20.6%[4].

However, the energy of the band gap exceeds the ideal range (1.4–1.5 eV), which could be a reason for the difficulty in achieving higher efficiency. Therefore, new PV materials have recently been identified as Bismuth chalcogenides (Bi-CAL) such as Bi_2S_3, Sb_2BiSe_3, $CuBiS_2$, and $AgBiS_2$ to fulfill world energy requirements [5, 6]. Bi_2S_3 is a promising material for future PV technology due to its high absorption coefficient (10^5 cm^{-1}) [1]. It normally shows n-type conductivity [2] but depending on the deposition techniques and temperature, it also exhibits p-type conductivity [7]. Its band gap is varied between 1.1 to 1.7 eV due to quantum confinement and/or variations in stoichiometry [1-3] and a larger absorption coefficient(10^5 cm^{-1})[8] compared to Sb_2S_3. Bi_2S_3 consists of Bismuth (Bi) and Sulfur(S), which is available in an abundant amount in earth's crust, making it economically viable [9]. Among others emerging PV technology Bi_2S_3 is a stable and non-toxic absorber layer [10, 11]. Due to its non-toxic properties, it is used in medicine products such as Pepto-Bismol [6]. Even if defects are present in Bi_2S_3, it has very good optoelectronics properties. Means it has very good defect tolerance. Bi_2S_3 unit cell structure is orthorhombic and its crystal structure consists of nano-ribbons bonded with Van der Waals forces. Which makes it defect tolerance at the grain boundary [12]. However, Bi_2S_3 has not received as much attention as a solar cell material in comparison to Sb_2S_3. Reported experimental efficiencies for Bi_2S_3-based solar cells are 1.57% [13], 3.2% [14] and 2.52% [24]. There are various methods for synthesizing Bi_2S_3 material, and all methods have their advantages and disadvantages [15]. To date, the highest Power conversion efficiency(PCE) reported for Bi_2S_3 thin film solar cells is 0.75%[16]. Apart from Bi_2S_3 thin film solar cells, Bi_2S_3 quantum dot-sensitized solar cells have a PCE of 3.1%[17], and the cross-linked heterostructure of Bi_2S_3/TiO_2 has the highest efficiency of 13.29 %%[18] and reported efficiency using SCAPS-1D is around 23%[19]

In this work, firstly, the Density of States (DOS), Electronic Band structure, and band gap of Bi_2S_3 absorber layer have been calculated using density functional theory(DFT) first principle computation framework by Quantum Espresso(QE) Burai[20]. Then the ITO/ETL/ Bi_2S_3/Au solar cell structure was designed, where CdS, ZnS, SnS_2 , and In_2S_3 were used as ETL layers in SCAPS-1D. The optimization has been made to know the best-suited ETL layer for Bi_2S_3 absorber layer using SCAPS-1D, as this process is time-consuming and highly expensive to study with all combinations experimentally. However, except for a few articles, Bi_2S_3 as an absorber layer of a solar cell has not been investigated much theoretically as compared to similar Sb_2S_3. Therefore, this study conducted with different ETL (CdS, ZnS, SnS_2, and In_2S_3) layers. To know the best ETL for Bi_2S_3 solar cell for the designed structure. After that, study the effect of thickness variation of absorber layer as well as ETL together, Shunt resistance(Rsh), Series Resistance(Rs) and temperature(T°K) on Short circuit current density(Jsc), Open circuit Voltage (Voc), Fill Factor(FF) and Efficiency along with their capacitance−voltage (C−V), band diagram, recombination rate, generation rate, quantum efficiency (QE), and J-V characteristics.

2. Numerical Simulations and Computational Study

2.1. Calculations of Bi_2S_3 material using DFT First-Principles

In this work, DFT-based computational studies were performed using Quantum ESPRESSO (QE) Burai 1.3 framework to optimize, and calculate the material's properties. In this methodology, the Perdew−Burke−Ernzerhof (PBE) framework was utilized to analyze the exchange-correlation interaction. The selection of exchange-correlation functionals (XCs) is important for the DFT calculation. The Broyden-Fletcher-Goldfarb-Shannon (BFGS) algorithm[21] was utilized with various XCs to determine the lowest energy configuration for the fully stable structure. The formation energy (ΔE_f, eV/ atom) of the optimized unit cell structure and its computed lattice parameters are primarily compared with the documented experimental findings. After comparison, the most accurate data provided by XC was used for the calculation of all Bi_2S_3 material properties. For the computational analysis of Bi_2S_3 material, the cutoff energy (Ecut) was set to 720 eV. For the SCF (Self-Consistent Field) calculation, a Monkhorst-Pack grid [22] of 6 × 6 × 6 (k-point) was used for Bi2S3 modeling. Conversely, a larger k-point mesh (8 × 8 × 8) was used to examine the electronic charge density map and the topology of the Fermi surface. In this set of calculations, a full energy value of 1×10^{-6} eV/atom was employed as the convergence tolerance for geometry optimization. The maximum potency applied to the atoms was 0.0249 eV/Å, while the largest allowable atomic displacement was 0.002 Å, and the upper limit for stress was 0.022 GPa.

2.2. Solar cell Simulation using SCAPS-1D

The study is supported using 1D solar cell capacitance software (SCAPS 1D), which was established by Mark Burgelman and his team at the University of Gent.[23] By putting suitable defect values, this software could provide efficiency near the experimental values. The mechanisms of light absorption, exciton production, transfer of charge and assembly, and recombination were all simulated by this program. Poisson's equation, which describes the relationship between electrostatic potential and charge density distribution, is defined by Equation (1).

$$\frac{d^2}{dx^2}\psi\,(x) = \frac{q}{\varepsilon_r\varepsilon_0}\,[p\,(x) - n\,(x) + N_D - N_A + \rho_p - \rho_n] \qquad (1)$$

where, ϵ_r = Relative permittivity, ϵ_0 = Permittivity of free space, ψ = Electric potential, N_D = Donor density, N_A = Acceptor density, ρ_p = Hole charge density, ρ_n = Electron charge density, n(x) and p(x) = electron and hole concentrations at position x. q = Electronic charge .

$$\frac{dn}{dt} = \frac{1}{q}\frac{\partial Jn}{\partial x} + (G_n - R_n) \qquad (2)$$

$$\frac{dp}{dt} = \frac{1}{q}\frac{\partial Jp}{\partial x} + (G_p - R_p) \qquad (3)$$

where, Jp = Holes current densities, Jn = Electrons current densities , Gp = Generation rate of holes, Gn = Generation rate of Electrons, , Rn = Electron recombination rate, Rp = Hole recombination rate. Both current density of electron and hole are computed using the charge carrier drift-diffusion equation which is given in Equations (4) and (5).

$$J_n = q\,\mu_n\,n\,E + q\,D_n\frac{dn}{dx} \qquad (4)$$

$$J_p = q\,\mu_p\,p\,E - q\,D_p\frac{dp}{dx} \qquad (5)$$

where, D_n = Diffusion constant of electron, D_p = Diffusion constant of hole, μ_n = Electron Mobility, μ_p =hole Mobility.

The Fill Factor(FF) can be calculated using Equation (6).

$$FF = \frac{J_{mp} \times V_{mp}}{J_{SC} \times V_{OC}} \qquad (6)$$

where, J_{mp} = Maximum computed current, V_{mp} = Maximum computed voltage, Jsc = Short circuit current, Voc = Open circuit voltage.

The device efficiency can be determined using Equation (7)

$$\eta = \frac{J_{SC} \times V_{OC} \times FF}{P_{in}} \qquad (7)$$

2.3. Bi_2S_3 Solar Cell Structure

The multi-layers Bi_2S_3 structure consists of ITO/ETL/ Bi_2S_3/Au as illustrated in in fig 1(a). Where Indium-doped tin oxide (ITO) was utilized as front contact, the ETL was utilized to transport electrons to the absorber and block holes, the Bi_2S_3 acted as the main layer of the solar cell, and there was a back metal contact. Figure 1(a) shows the Bi_2S_3-based solar cell structure that was designed for this study. Where the ETL layer was (CdS, ZnS, SnS_2 , In_2S_3), Bi_2S_3 was used as an absorber layer, and gold (Au) was used as a back metal contact. There were four ETLs studied in this paper to find out the best structure for each ETL. Tables 1 and 2 show the input parameters of different layers and the Bi_2S_3/ETL interface.

Table 1 Material parameters of different layers used for the simulation

Material property	Bi_2S_3	ITO	CdS	SnS_2	ZnS	In_2S_3
Thickness [nm]	1.5(Optimized)	500	40(Optimized)	40(Optimized)	40(Optimized)	40(Optimized)
Bandgap, Eg [eV]	1.25(calculated)	3.5	2.42	1.85	3.3	2.5
Electron affinity, X [eV]	4.58	4	4.2	4.26	4.4	4.25
Relative dielectric permittivity, (ε_r)	13.6	9	9.35	17.7	10	7.72
Conduction band effective DOS N_C(cm^{-3})	2.20×10^{18}	2.20×10^{18}	2.20×10^{18}	7.320×10^{18}	2.2×10^{18}	2.2×10^{18}
Valence band effective DOS N_V(cm^{-3})	1.80×10^{19}	1.80×10^{19}	1.80×10^{19}	1.0×10^{19}	1.8×10^{19}	1.8×10^{19}
Electron thermal velocity (cm s^{-1})	1×10^7	1×10^7	1×10^7	1×10^7	1×10^7	1×10^7
Hole thermal velocity (cm s^{-1})	1 × 107	1×10^7	1 × 107	1 × 107	1×10^7	1×10^7
Electron mobility, μn (cm^2 $V^{-1}S^{-1}$)	1100	20	100	50	100	100
Hole mobility, μh (cm^2 $V^{-1}S^{-1}$)	200	10	25	25	25	25
Donor density, ND (cm^{-3})	0	1.0×10^{21}	1.150×10^{17}	1×10^{17}	1×10^{17}	1×10^{17}
Acceptor density, NA (cm^{-3})	2.0×10^{16}	0	0	0	0	0
Total Defect density (cm^{-3})	1×10^{14}	1×10^{14}	1×10^{16}	1×10^{15}	1×10^{15}	1×10^{15}
References	[24]	[25]	[26]	[27]	[28]	[29]

Table 2 Interface parameters of the solar cell

Interface	Defect type	Capture Cross Section: Electrons/holes [cm^2]	Energetic Distribution	Reference for defect energy level	Total density [cm^{-2} (integrated over all energies)
Bi_2S_3/ETL	Neutral	1.0×10^{-17} and 1.0×10^{-18}	Single	Above the VB maximum	1.0×10^{10}

3. Results and discussion

3.1. Analysis of DFT Results

3.1.1. Structural Properties of the Bi_2S_3 Compound.

The Bi_2S_3 absorber layer crystal structure is Orthorhombic P with Pnma space group (no. 62) is illustrated in Fig 1(b). The crystal arrangement of Bi_2S_3 is composed of five distinct atoms having two unique Bi positions and three unique S positions. Each Bi atom is connected to seven S atoms. Three of the S atoms are bonded to the Bi atom via short distances, while the remaining four S atoms are connected through longer distances. The Bi–S short-bonds created a tightly bonded ribbon, whereas the Bi–S long-bonds established a Van der Waals force, leading to a weak interaction among the aligned ribbons. The determined lattice parameter of the best-optimized structure for Bi_2S_3 were, a =11.741 Å, b= 4.053 Å and c = 11.139 Å, which aligns very well with the experimental data (a= 11.305 Å b= 3.981 Å and c= 11.147 Å)[30]. The very consistent lattice parameters and negative formation energy (−21893.47 eV/atom) indicate the stability of Bi_2S_3, which is very important for the solar cell absorber material.

3.1.2. DOS and Band Structure of Bi_2S_3 absorber layer

The electronic band structure and the associated density of states (DOS) for the Bi_2S_3 absorber layer are illustrated in fig.1(c) and (d). The Fermi level (E_F) in the fig 1(d) is shown by a horizontal red dotted line. The bands that have values more than E_F are called conduction bands, and those bands that have values less than E_F are called valance bands. It is seen that neither bands cross the Fermi level nor do they interfere with each other.

So, this compound has a bandgap, and the bandgap nature is indirect as the valence band maximum (VBM) and the conduction band minimum (CBM) are located around Z point and between Γ-Y direction. The calculated value of the bandgap is 1.25 eV, which has been obtained by the Perdew-Burke-Ernzerhof (PBE) technique. This observed value is within the ranges of other earlier calculations experimentally 1.26 eV[31] and 1.360 eV[32]. Theoretically 1.22 eV[33] and 1.38 eV[30]. The VBM (valence band maxima) is closest to the Fermi level and crossing nature of total density of states (TDOS) at E_F confirming the p-type carriers with semiconductor behavior.

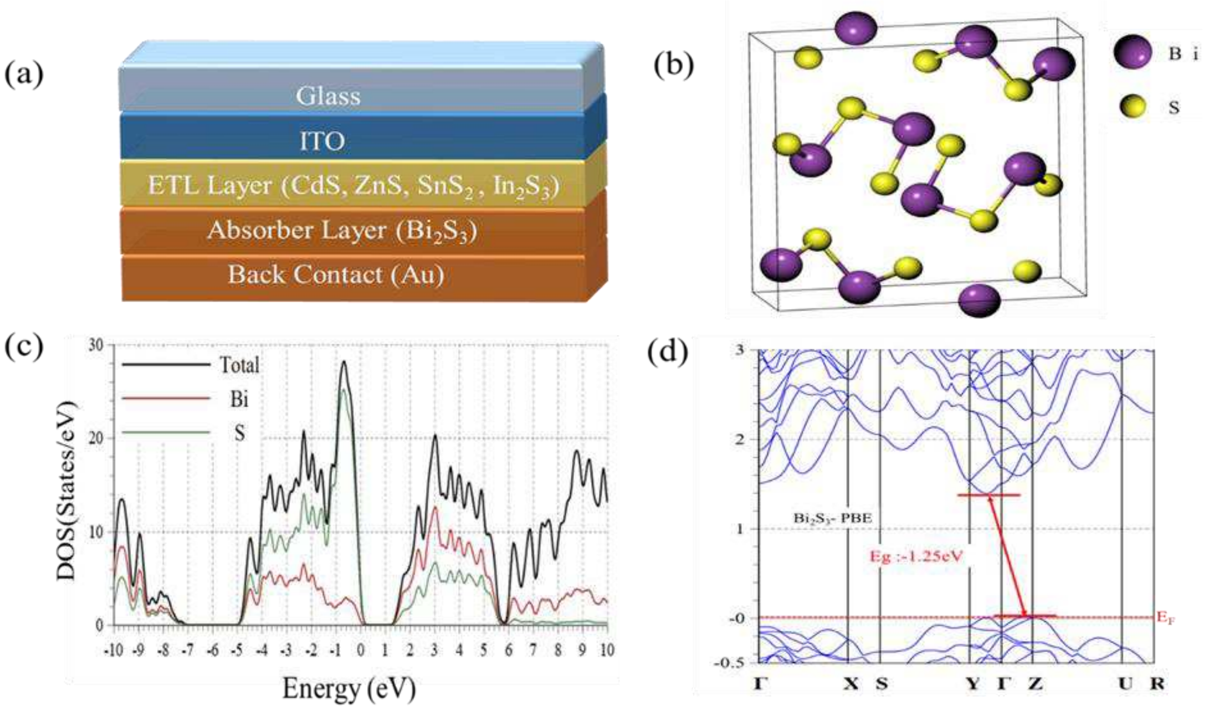

Fig 1 a) Structure of the Bi_2S_3-based Solar cell, b) the 3D construction of the Bi_2S_3, (c) Band structure, and d) DOS of Bi_2S_3

3.2. Analysis of SCAPS-1D Results

3.2.1. Effect of ETL and absorber layer thickness Variation

In fig 5(a to d) indicates the effect of ETL (CdS, ZnS, SnS_2 and In_2S_3) and absorber layer thickness variation on the open circuit voltage(Voc), Short Circuit Current Density(Jsc), Fill Factor(FF) and Efficiency. Absorber layer thickness is varied from 0.5 to 2.5 µm and ETL layer thickness is varied from 20 to 100nm for best ETL layer among four for Bi_2S_3 absorber layers. Voc is maximum between 0.5 to 1.2µm of absorber layer thickness and it almost constant through of the ETL layer thickness (20nm to 100nm) variation. If absorber layer thickness is higher than 1.1 µm, Voc gradually decreasing. The maximum Voc is 839.7 mV when CdS is used as ETL . In case of Jsc, the maximum value is almost same for all ETL but maximum Jsc observed between 1.25 to 2 µm of Bi_2S_3 thickness. The maximum Fill Factor of the solar cell is around 82.48% with ZnS and SnS_2 as ETL with absorber layer between 0.5 to 0.8µm. The maximum fill factor is 82.42 % with CdS as ETL with its thickness between 20 to 30 nm and absorber layer thickness between 0.5 to 0.8µm. When In_2S_3 is considered as ETL layer then the maximum Fill Factor is 82.47 % with In_2S_3 its thickness between 20 to 50nm and absorber layer thickness is around 0.5 to 0.6 µm. In case of efficiency, if ZnS as ETL the maximum efficiency between 25.05% to 25.27 %. The maximum efficiency with SnS_2 and In_2S_3 as ETL having same maximum between efficiency 25.04 to 25.26 % and with CdS as ETL having maximum efficiency between 25.02% to 25.25 % . The efficiency of the simulated solar cell is almost constant throughout the ETL thickness (20 nm to 100 nm) and it is maximum if absorber layer thickness is greater than 1.2µm. So for the other analysis thickness of the Bi_2S_3 absorber layer was fixed at 1.5 µm.

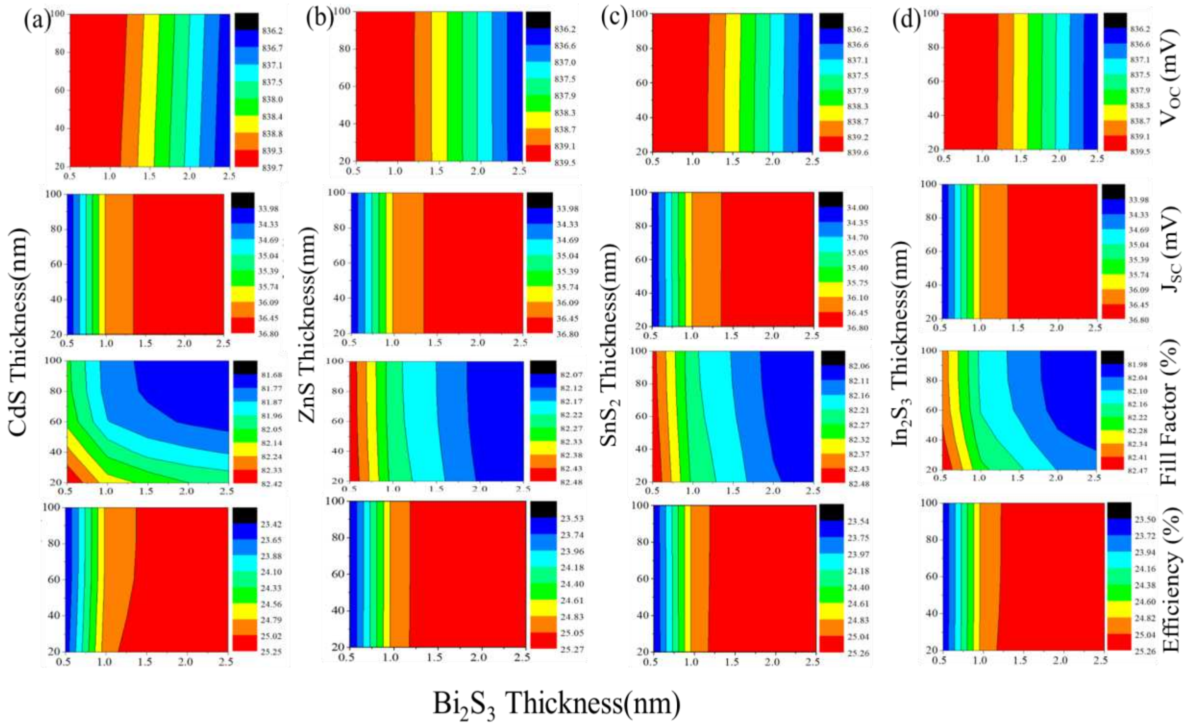

Fig 2 Contour plots shows the Bi2S3 and ETL((a) CdS, (b)ZnS (c) SnS_2 and (d) In_2S_3) thickness variation on Voc, Jsc Fill Factor and Efficiency

3.2.2. Bi_2S_3 Energy Band Diagram (EBD)

The ETL, play vital roles in the impact of the conduction band (CB)/valence band (VB) offset of the EBD of Bi_2S_3 solar cell. The energy level of the materials in Bi_2S_3 has an enormous impact on the efficiency. In Bi_2S_3, electrons are infused to ETL CB. In ITO and Au, electrons and holes are collected simultaneously. Fig 4(a) to (d) shows the EBD for the structure of ITO/CdS/Bi_2S_3/Au, ITO/ZnS/ Bi_2S_3/Au, ITO/SnS_2/Bi_2S_3/Au, and ITO/In_2S_3/Bi_2S_3/Au respectively. In thermal equilibrium state, the Fermi level remains consistent throughout the device structure. However, the introduction of photons into the device disrupts this alignment, resulting in the formation of quasi-Fermi energy levels. From all four figures, it can be seen that the small CBO of the Bi_2S_3 /ETL interface, it helps electrons to move easily which results in higher and almost same efficiency for all four devices.

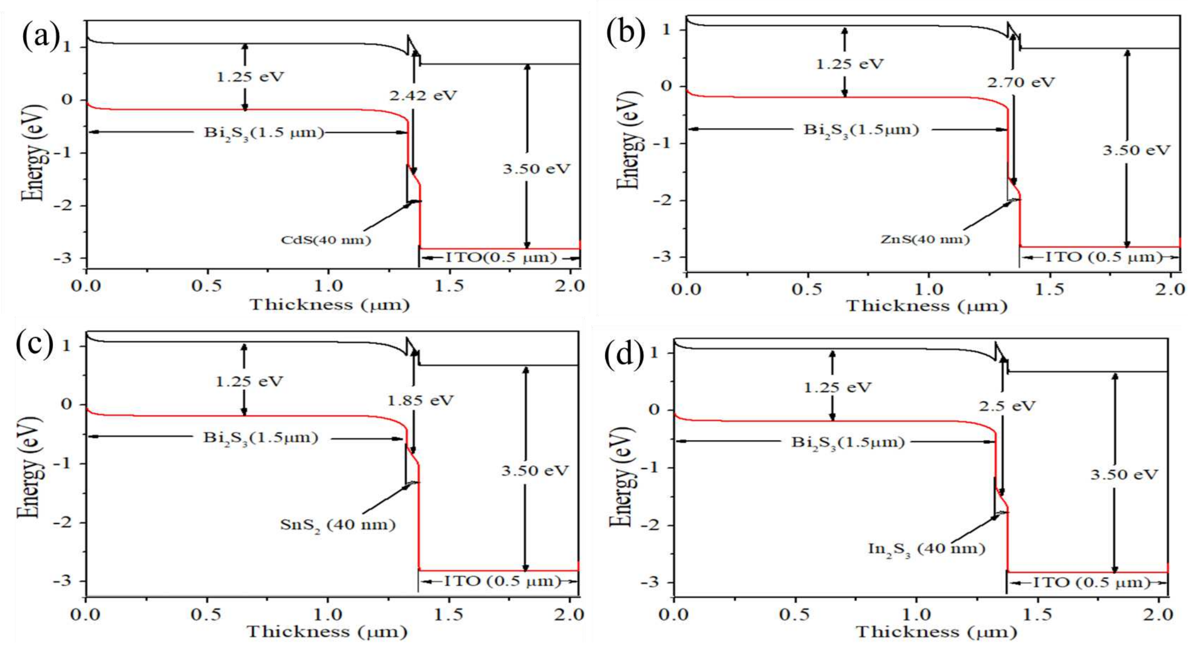

Fig 3 Energy Band Diagram of Bi_2S_3 based solar cell with different ETLs (a) CdS, (b) ZnS (c) SnS_2 and (d) In_2S_3

3.2.3. Effect of Series Resistance

As Series(Rs) and shunt(Rsh) resistance play very crucial role on shape of the current voltage characteristics of solar cell. The performance Bi_2S_3 based solar cell is also very important to know the effect of Rs and Rsh which are largely formed by relation between structures' different layers, metal contacts, the semiconductor-metal interface, and improper solar cell processing processes[34]. To know the effect of Rs on the Bi_2S_3 solar cell parameters the Rs value varied from 0 to 10 Ω-cm^2 at the $10^6\Omega$-cm^2 shown in fig 4 (b). From the figure it can observed that there is small change in Jsc and V_{OC} but fill factor decreased by very high value (for Zns 82.25% to 48.64 %) with all the four ETL of Bi_2S_3 solar cell. The JV characteristics of a heterojunction SC are shown in a typical diode model as Equation (8) [35].

$$J = J_L - J_0\left[\exp\left(\frac{e(V+J\times Rs)}{AK_BT}\right) - 1\right] - \frac{(V+J\times Rs)}{R_{sh}} \quad (8)$$

where, J = Circuit current, J_L = Current induced from light absorbance, V = Voltage, J_0 = Reverse saturation current, A = Ideality factor, e = Charge of electron, K_B = Boltzmann constant, Rs = Series resistance, Rsh = Shunt resistance, T = Temperature.

3.2.4. Effect of Shunt Resistance(Rsh)

Rsh variation on Au/Bi_2S_3/ ETL (CdS, ZnS, SnS_2 and In_2S_3/ITO based solar cell on the Short Circuit Current Density(Jsc), open circuit voltage(Voc), Efficiency and Fill Factor(FF). The Rsh value is varied from 10 Ω to 10^7 Ω-cm^2 during simulation. But in figure, Rsh is varied form 10^3 Ω to 10^7 Ω-cm^2 to get clear difference on solar cell parameters with different ETL layer. From the figure it can be observed that simulated solar cell parameters gradually increasing with increase in shunt resistance up to 10^5 Ω-cm^2 . After that there is no change in solar cell parameter with further increase in Rsh. This may due to p-n junction follow the low resistance channel for junction current flow after specific Rsh solar cell parameters reached in to saturation. The major variation occurred while ZnS used as ETL layer as its PCE increased from 2.97 % to 25. 21 %. So high value of Rsh helps the Bi_2S_3 to provide high efficiency.

3.2.5. Effect of Temperature

Effect of temperature on solar cell parameters have drawn a lot of interest on by PV industries. Still, they demonstrate thermal instability when expose light on to solar cells[36]. The solar cell efficiency may be decreased significantly while remained expose for long time at higher temperatures[37].So observation of temperature effect on Bi_2S_3 solar cell is needed.To observe the temperature effect of the Bi_2S_3 solar cell parameters, temperature is varied from 300° K to 450° K shown in figure 11(c). It can be observed that Voc is decreased by significant amount with increase in temperature for all devices. It may due to increase in reverse saturation current with temperature in the device. The impact of temperature can be analyze using equation (9) and (10).

$$\mathrm{Voc} = \frac{nKT}{q} \log \left(\frac{J_{SC}}{J_0} + 1\right) \qquad (9)$$

$$\frac{dV_{OC}}{dT} = \frac{V_{OC}}{T} - \frac{E_g/q}{T} \qquad (10)$$

where, J_0 = Reverse saturation current, T = Temperature, E_g = Bandgap, q = Electronic charge, n = ideality factor, K = Boltzmann constant.

The Jsc is not much effected by increase in temperature but FF and efficiency are decreased by significant percentage in all the devices.

3.2.6. Effect of Generation and Recombination Rate

For the generation rate calculation SCAPS 1D uses equation (11) by considering the contribution of electron-hole pairs for each position and spectral region.

$$G(\lambda, x) = \alpha(\lambda, x) \times N_{phot}(\lambda, x) \qquad (11)$$

where, $N_{phot}(\lambda, x)$ = Photon flux

The generation rate of electron and holes with respect to position for with different ETL shown in figure 12(a). it can be observed that maximum generation achieved around 1µm position. The maximum generation rate (1.54×10^{22} cm^3 s^{-1}) at 1µm position for ZnS and In_2S_3 electron transport layer. The recombination rate is actually opposite to the generation rate as it reduces photo-current by recombining electron hole pairs. Figure 12(b) shows the recombination rates for four structures where it can be seen that recombination of electron hole pairs increases exponentially between 0 to 0.15 µm up to 2.52×10^{20} cm^3 s^{-1} and constant up to 0.8µm again exponentially increases and reach up to maximum recombination(1.14×10^{21} cm^3 s^{-1}) around 0.9 µm after that it sharply decline and becomes minimum at 1 µm. The recombination rate is almost same for all device structure. The charge carriers' density and carrier life time have an effect on the recombination rate in solar cell. The increase in electron-hole recombination is caused by defect states at the interfaces and in the absorber layer.

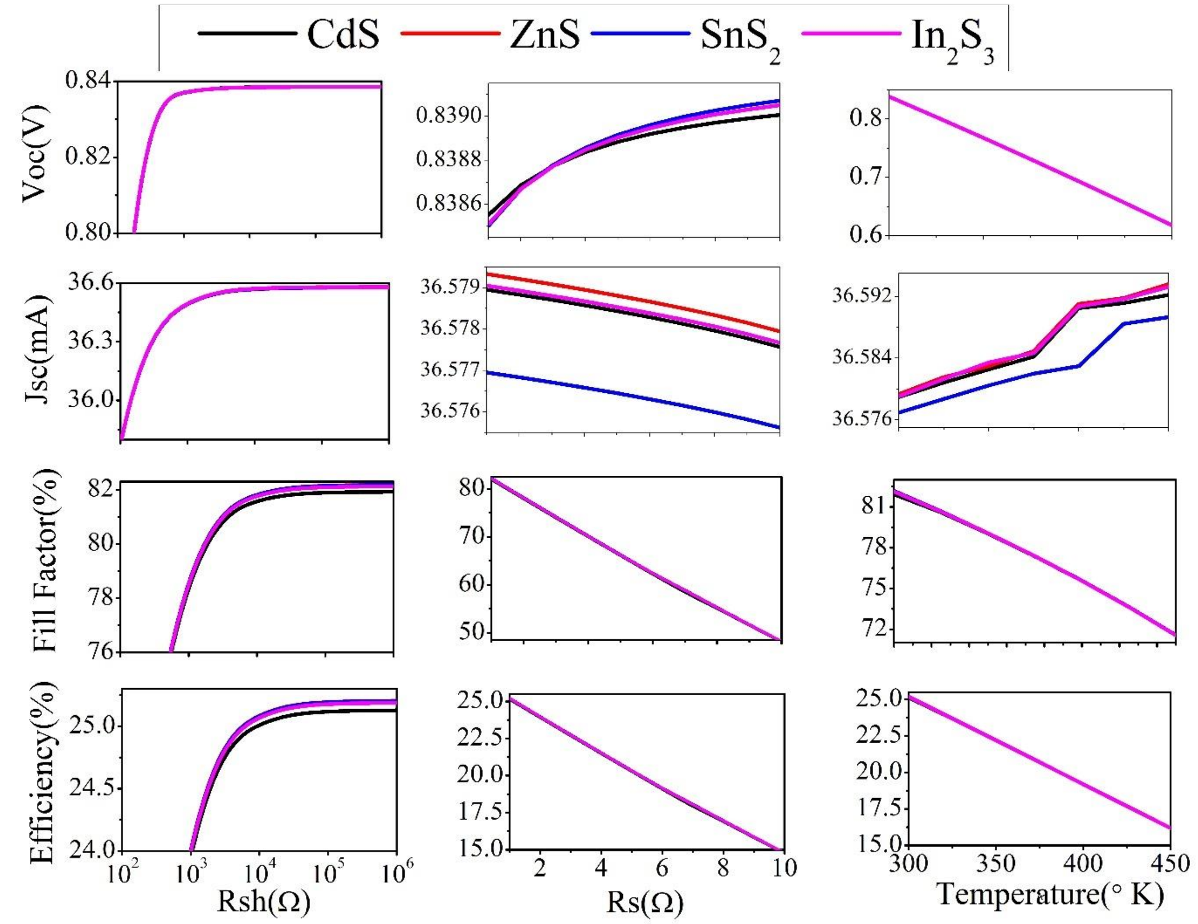

Fig 4 Effect on Voc, Jsc, Fill Factor and Efficiency with different ETLs with the variation of a) series resistance, b) shunt resistance, and c) temperature.

3.2.7. Capacitance and Mott−Schottky Analysis

Capacitance and Mott−Schottky curve shown in figure 5(c) and (d). when the voltage was increased from −0.4 to 0.8 V for all the devices at fixed frequency (1 MHz). The capacitance gradually increases from 35 nF/cm² with applied voltage and reach its maximum value around 65-68 nF/cm² for applied voltage around 0.7V. lower capacitance at initial position indicates the fully depleted region in Bi_2S_3 near Au interface. Increase in capacitance with position specify the narrowing the depletion may due to increase in carrier accumulation. Mott−Schottky (MS) law is exclusively used for PN junction characteristics. The MS plot is generally used for the built in potential(Vbi) and carrier concentration calculation. Linear region of the plot shows the proper PN junction formation. The x-axis intersection of the MS plot slope provide the Vbi which is important for the interpretation of the electric field. With increase in applied voltage the MS value is decreases for each ETL in the device which is similar to the reported result.

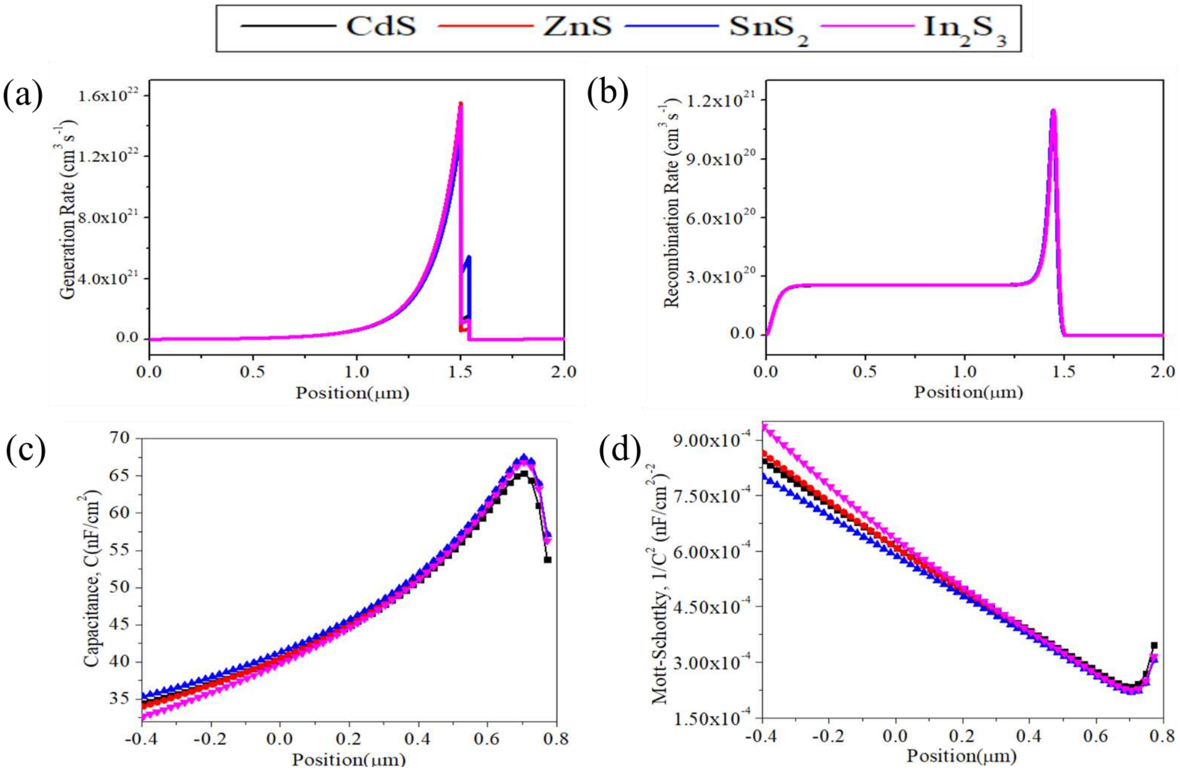

Fig 5 (a) Generation rate, (b) recombination rate , (c) Capacitance and (d)Mott-Schottky of Bi2S3 based solar cell with different ETLs

3.2.8 Efficiency of the device after optimization

After optimization of various solar cell parameters, the device efficiencies are presented in Table 3. Among the different ETLs, ZnS yielded the highest efficiency; however, the differences in efficiency among the other ETLs are relatively small. The previously reported theoretical efficiency was 24.05%[18]. In this work Jsc and FF is improved as compared to previously reported work. The quantum efficiency (QE) and current–voltage (J–V) characteristics are shown in Figure 6(a) and 6(b), respectively. The QE and J–V curves are nearly identical for all ETLs due to the minimal variation in efficiency. The QE response extends up to 1000 nm, which is highly favorable for practical applications.

Table-3 Comparison of PV Parameters of Bi_2S_3 Based Solar Cells

Type	Device Structure	Voc(V)	Jsc(mA/cm^2)	FF(%)	Eff(%)	Year	ref
T	FTO/SnO_2/CdS/ Bi_2S_3/ Spiro OMeTAD/Au	1.02	32.18	73.01	24.05	2024	[18]
T	FTO/CdS/ Bi_2S_3/ Spiro OMeTAD/Au	1.02	31.13	73.05	23.05	2024	[18]
T	ITO/CdS/ Bi_2S_3/Au	0.8386	36.5789	81.93	25.13	Present	
T	ITO/ZnS/ Bi_2S_3/Au	0.8385	36.5793	82.18	25.21	Present	
T	ITO/SnS_2/ Bi_2S_3/Au	0.8385	36.5769	82.18	25.20	Present	
T	ITO/In_2S_3/ Bi_2S_3/Au	0.8385	36.5790	82.12	25.19	Present	

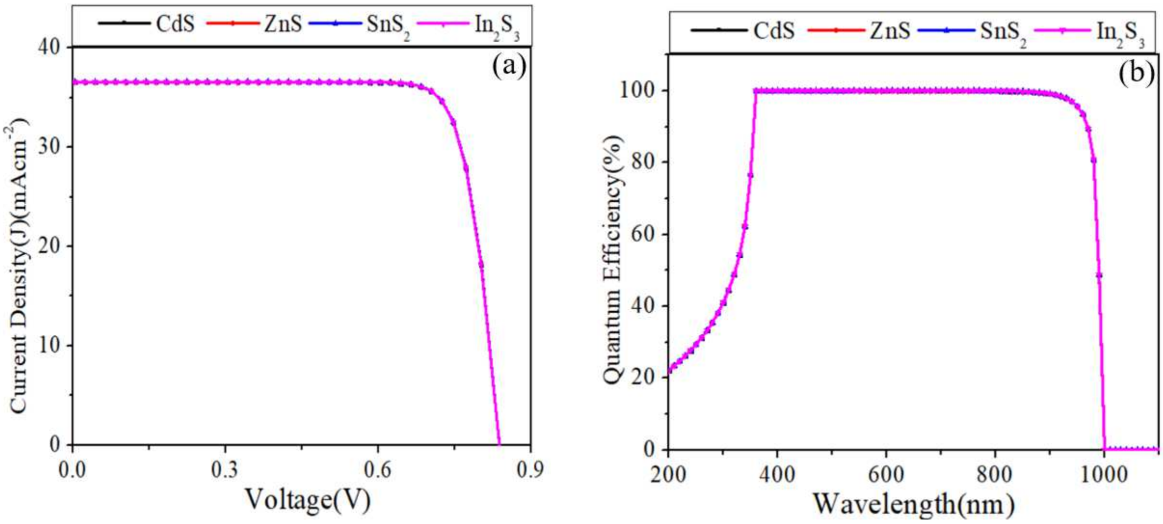

Fig 6 (a)J-V curve and (b) QE curve of ITO/ETL/ Bi2S3/Au solar cell with different ETLs

Conclusion

After optimization of Bi_2S_3, the density of states (DOS), electronic band structure, and band gap were calculated using density functional theory (DFT). Bi_2S_3 exhibits p-type indirect band gap behavior with a band gap of 1.25 eV.A Bi_2S_3-based solar cell was simulated using SCAPS-1D in the structure Au/Bi_2S_3/ETL/ITO, where the electron transport layers (ETLs) considered were CdS, ZnS, SnS_2, and In_2S_3. The study investigated the effects of absorber and ETL thickness variations, shunt resistance (Rsh), series resistance (Rs), operating temperature, band gap structure, capacitance, and generation and recombination rates.

The optimized absorber layer thickness was found to be 1.5 µm, while the optimal ETL thickness was 40 nm. Under these conditions, the highest power conversion efficiency (PCE) of 25.21% was achieved using ZnS as the ETL. The optimized values for Rs and Rsh were approximately 1 Ω and 105 Ω, respectively. It was observed that efficiency sharply decreases when the operating temperature exceeds room temperature. The generation rate peaked at an absorber thickness of 1.5 µm, while the recombination rate was highest at 1.43 µm.

This study highlights the influence of thickness, series and shunt resistances, and temperature on the efficiency of Bi_2S_3 solar cells, as well as on their generation and recombination behavior. The J–V and quantum efficiency (QE) characteristics further confirm the performance of the Bi_2S_3-based solar cell, offering insights that may support future experimental research.

Data and code availability

The data supporting the findings of this study are available in the main text and supplementary Information.

Acknowledgement

The authors would like to thank Quantum ESPRESSO Foundation for providing QE with BURAI as GUI for optimization and band gap estimation and Marc Burgelman, ELSI, University of Gent, Belgium for providing the SCAPS simulation software (Version: SCAPS3311).

Conflict of interest

The authors declare that they have no conflict of interest and no support of funding for their research and/or manuscript preparation.

Author Contributions

Vishvas Kumar has done investigation, visualization, optimization, simulation, writing and editing of the manuscript.

References

[1] M. Green, M.A., Dunlop, E.D., Levi, D.H., Hohl-Ebinger, J., Yoshita, M., Ho-Baillie, A.W. "Solar cell efficiency tables (version 54)" Prog. Photovolt. Res. Appl., 27, 565–575 (2019).

[2] G. Konstantatos, L. Levina, J. Tang, E.H. Sargent, "Sensitive Solution-Processed Bi_2S_3 Nanocrystalline Photodetectors", Nano Lett., 8, 4002–4006 (2008).

[3] S.Y. Wang, et al., "A novel multi-sulfur source collaborative chemical bath deposition technology enables 8%-efficiency Sb_2S_3 planar solar cells", Adv. Mater., 34, 2206242 (2022).

[4] M. Courel, T. Jiménez, A. Arce-Plaza, D. Seuret-Jiménez, J.P. Morán-Lázaro, F.J. Sánchez-Rodríguez, "A theoretical study on Sb_2S_3 solar cells: The path to overcome the efficiency barrier of 8%", Sol. Energy Mater. Sol. Cells, 201, 110123 (2019).

[5] N.C. Miller, M. Bernechea, "Research Update: Bismuth-based materials for photovoltaics", APL Mater., 6, 084503 (2018).

[6] A. Zakutayev, "Brief review of emerging photovoltaic absorbers", Curr. Opin. Green Sustain. Chem., 4, 8–15 (2017).

[7] N. Mahuli, D. Saha, S.K. Sarkar, "Atomic layer deposition of p-type Bi_2S_3", J. Phys. Chem. C, 121, 8136–8144 (2017).

[8] M. Su, Z. Feng, H. Chen, X. Liu, J. Wen, H. Liu, "Efficient SnO_2/CdS double electron transport layer for Sb_2S_3 film solar cell", J. Alloy Compd., 882, 160707 (2021).

[9] C. Wadia, A.P. Alivisatos, D.M. Kammen, "Materials availability expands the opportunity for large-scale photovoltaics deployment", Environ. Sci. Technol., 43, 2072–2077 (2009).

[10] P.C.K. Vesborg, T.F. Jaramillo, "Addressing the terawatt challenge: scalability in the supply of chemical elements for renewable energy", RSC Adv., 2, 7933–7947 (2012).

[11] R. Mohan, "Green bismuth", Nat. Chem., 2, 336 (2010).

[12] R.E. Brandt, V. Stevanović, D.S. Ginley, T. Buonassisi, "Identifying defect-tolerant semiconductors with high minority-carrier lifetimes: beyond hybrid lead halide perovskites", MRS Commun., 5, 265–275 (2015).

[13] C. Rosiles-Perez, S. Sidhik, L. Ixtilico-Cortés, F. Robles-Montes, T. López-Luke, A.E. Jiménez-González, "High short-circuit current density in a nontoxic Bi_2S_3 quantum dot sensitized solar cell", Mater. Today Energy, 21, 100783 (2021).

[14] J. PI, G. Vignesh, S. Vijaya, S. Anandan, N.K.P. Ramachandran, "Enhancing the power conversion efficiency of $SrTiO_3$/CdS/Bi_2S_3 quantum dot-based solar cell using phosphor", Appl. Surf. Sci., 494, 551–560 (2019).

[15] T.O. Ajiboye, D.C. Onwudiwe, "Bismuth sulfide-based compounds, properties, synthesis, and applications", Results Chem., 3, 100151 (2021).

[16] H. Song, X. Zhan, D. Li, Y. Zhou, B. Yang, K. Zeng, J. Zhong, X. Miao, J. Tang, "Rapid thermal evaporation of Bi_2S_3 layer for thin film photovoltaics", Sol. Energy Mater. Sol. Cells, 146, 1–7 (2016).

[17] A.S. Rasal, K. Dehvari, G. Getachew, C. Korupalli, A.V. Ghule, J.Y. Chang, "Efficient quantum dot-sensitized solar cells through sulfur-rich carbon nitride modified electrolytes", Nanoscale, 13, 5730 (2021).

[18] S. Mathur, V. Bishop, A. Swindle, W. Wei, "Enhanced performance of Bi_2S_3/TiO_2 heterostructure composite films for solar cell applications", J. Photochem. Photobiol., 25, 100256 (2025).

[19] M.A. Saifee, U. Latief, J. Ali, et al., "Tri-chalcogenides (Sb_2S_3/Bi_2S_3) solar cells with double electron transport layers: design and simulation", Discov. Energy, 4, 4 (2024).

[20] P. Giannozzi et al., J. Phys.:Condens. Matter 21 395502 (2009).

[21]T.H. Fischer, J. Almlof, "General methods for geometry and wave function optimization", J. Phys. Chem., 96, 9768 (1992).

[22] H.J. Monkhorst, J.D. Pack, "Special Points for Brillouin-Zone Integrations", Phys. Rev. B, 13, 5188–5192 (1976).

[23] K. Decock, A. Niemegeers, J. Verschraegen, "SCAPS Manual Most Recent", Univ. Gent, (2021).

[24] S. Das, E. Riefe, S. McWhorter, "Device design and photovoltaic performance of heterojunction solar cells using ultra-thin Bi_2S_3 photoabsorber", IEEE 13th Nanotechnol. Mater. Devices Conf. (NMDC), IEEE, Portland, 1–4 (2018).

[25]M.K. Hossain, M.H.K. Rubel, G.F.I. Toki, I. Alam, M.F. Rahman, H. Bencherif, "Effect of Various Electron and Hole Transport Layers on the Performance of $CsPbI_3$-Based Perovskite Solar Cells: A Numerical Investigation in DFT, SCAPS-1D, and wxAMPS Frameworks", ACS Omega, 7, 43210–43230 (2022).

[26] A. El Kissani, H.A. Dads, S. Oucharrou, F. Welatta, H. Elaakib, L. Nkhaili, A. Narjis, A. Khalfi, K. El Assail, A. Outzourhit, "Facile route for synthesis of cadmium sulfide thin films", Thin Solid Films, 664, 66–69 (2018).

[27] M. Haghighi, M. Minbashi, N. Taghavinia, D.H. Kim, S.M. Mahdavi, A.A. Kordbacheh, "A modeling study on utilizing SnS_2 as the buffer layer of CZT(S, Se) solar cells", Sol. Energy, 167, 165–171 (2018).

[28]A. Cherouana, R. Labbani, "Study of CZTS and CZTSSe solar cells for buffer layers selection", Appl. Surf. Sci., 424, 251–255 (2017).

[29] A. Rahmoune, O. Babahani, "Numerical analysis of Al/Gr/ETL/MoS_2/Sb_2S_3/Ni solar cell using non-toxic In_2S_3/SnS_2/ZnSe electron transport layer", Optik, 283, 170875 (2023).

[30] R. Caracas, X. Gonze, "First-principles study of the electronic properties of A_2B_3 minerals, with A=Bi, Sb and B=S,Se", Phys. Chem. Miner., 32, 295–300 (2005).

[31] Y. Chen, D. Wang, Y. Zhou, Q. Pang, J. Shao, G. Wang, J. Wang, L.D. Zhao, "Enhancing the thermoelectric performance of Bi_2S_3: a promising earth-abundant thermoelectric material," Front. Phys., 14, 13601 (2019).

[32] H. Cheng, B. Huang, J. Lu, Z. Wang, B. Xu, X. Qin, X. Zhang, Y. Dai, "Synergistic effect of crystal and electronic structures on the visible-light-driven photocatalytic performances of Bi_2O_3 polymorphs," Phys. Chem. Chem. Phys., 12, 15468–15475 (2010).

[33] D. Guo, C. Hu, C. Zhang, "First-principles study on doping and temperature dependence of thermoelectric property of Bi_2S_3 thermoelectric material," Mater. Res. Bull., 48, 1984–1988 (2013).

[34] M.T. Islam, A.K. Thakur, "Two-stage modelling of solar photovoltaic cells based on Sb_2S_3 absorber with three distinct buffer combinations," Solar Energy, 202, 304–315 (2020).

[35] Y. Li, B. Ding, Q.-Q. Chu, G.-J. Yang, M. Wang, C.-X. Li, C.-J. Li, "Ultra-high open-circuit voltage of perovskite solar cells induced by nucleation thermodynamics on rough substrates," Sci. Rep., 7, 46141 (2017).

[36] P. Holzhey, M. Saliba, "A full overview of international standards assessing the long-term stability of perovskite solar cells," J. Mater. Chem. A, 6, 21794–21808 (2018).

[37] R. Roesch, T. Faber, E. von Hauff, T.M. Brown, M. Lira-Cantu, H. Hoppe, "Procedures and practices for evaluating thin-film solar cell stability," Adv. Energy Mater., 5, 1501407 (2015).

Supplementary Files

This is a list of supplementary files associated with this preprint. Click to download.

- SupplementryMaterials.docx